Am J Transl Res 2023;15(5):3203-3216
www.ajtr.org /ISSN:1943-8141/AJTR0147254

Original Article

Mesenchymal stem cell-derived exosomes ameliorate TGF-β1-induced endometrial fibrosis by altering their miRNA profile

Limei Zhou*, Lan Dong*, Hengxing Li, Hua Liu, Jing Yang, Zhixin Huang

*Department of Obstetrics and Gynecology, Renmin Hospital of Wuhan University, Wuhan 430060, Hubei, China. *Co-first authors.*

Received October 25, 2022; Accepted March 1, 2023; Epub May 15, 2023; Published May 30, 2023

Abstract: Objective: Mesenchymal stem cell (MSC)-derived exosomes (MSC-exo) can treat reproductive disorders. However, the action of microRNAs (miRNAs) in this mechanism has yet to be systematically investigated. This study aimed to explore the effect of MSC-exo on TGF-β1-induced endometrial fibrosis in intrauterine adhesions and elucidate the regulatory mechanisms involved in key genes by comparing miRNA expression profiles. Methods: MSC-exo were isolated and identified based on particle size and protein marker detection. Cell counting kit-8, flow cytometry, and western blotting were used to determine the effects of MSC-exo on cell function and fibrosis in human endometrial epithelial cells (hEECs). Subsequently, we sequenced and annotated the small RNA in MSC-exo and TGF-β1-induced MSC-exo to screen for differentially expressed (DE) miRNAs. After the prediction and functional enrichment of target genes of DE miRNAs, key genes were selected for functional experiments. Results: TGF-β1 inhibited the proliferation of hEECs and promoted apoptosis and fibrosis. However, these effects were significantly reversed by the addition of MSC and MSC-exo. Fifteen DE miRNAs were identified by comparing the miRNA profiles of MSC-exo and TGF-β1-induced MSC-exo. Among these, miR-145-5p was found to be significantly upregulated in TGF-β1-induced MSC-exo. Furthermore, the addition of miR-145-5p mimic was found to reverse fibrosis in hEECs while promoting the expression of key autophagy protein P62. Conclusion: MSC-exo ameliorated TGF-β1-induced endometrial fibrosis. RNA sequencing, bioinformatic analysis, and functional experiments revealed that miR-145-5p may exert its action through the P62-dependent autophagy pathway.

Keywords: Intrauterine adhesion, endometrial fibrosis, mesenchymal stem cell-derived exosomes, RNA-sequencing, miRNA

Introduction

Intrauterine adhesion (IUA), also known as Asherman syndrome, is a uterine disorder characterized by scarring and adhesions in the pelvic or uterine cavities. Its clinical manifestations include abnormal menstruation, recurrent abortion, and secondary infertility accompanied by placental abnormalities, intrauterine growth restriction, and other pregnancy complications [1, 2]. The histologic appearance of IUA is endometrial fibrosis, in which most interstitial cells are replaced by avascular fibrous tissue and spindle myofibroblasts [3]. Possible mechanisms for triggering IUA include hypoxic injury, inflammatory response, decreased angiogenesis, disturbance of immune mechanisms, unregulated epithelial-mesenchymal transition (EMT), abnormal myofibroblast differentiation, abnormal stem cell regeneration, and disrupted proliferation of normal endometrial cells [4]. With the development and popularization of ultrasound and hysteroscopy, the number of diagnosed IUAs is increasing worldwide, wherein the estimated incidence varies from 2.2% to 40% depending on the type of intrauterine surgery patients have previously undergone [5]. In addition to these iatrogenic predisposing factors, different genetic profiles have been observed between IUA and non-IUA patients, indicating that genetic susceptibility is also a risk factor for IUA [6]. Therefore, under-

standing endometrial fibrosis from the perspective of the patient genetic background is important for interpreting the pathogenesis of IUA.

Mesenchymal stem cells (MSCs) have become the focus of IUA research due to their ability to regulate cell differentiation and proliferation, as well as inflammatory processes, oxidative stress, and angiogenesis [7]. However, their possible tumorigenicity, low infusion, and low retention limit their clinical application. In contrast, MSC-derived exosomes (MSC-exo) exhibit similar functions as their parental cells and are promising substitutes [8]. Exosomes are MSC-derived nanoscale extracellular vesicles (30-200 nm) that can release contents into the extracellular environment after fusion with the plasma membrane and play biological roles in the paracrine and endocrine pathways [9, 10]. Furthermore, evidence also indicates that the therapeutic effect of MSCs is mainly derived from paracrine factors secreted by MSC-exo [11]. Functional mediators of exosomes include cytokines, chemokines, mRNAs, and microRNAs (miRNAs) that mediate intercellular communication, immune regulation, and cell signal transduction [12, 13]. The miRNA expression profile of exosomes differs from that of parental cells, thus playing a role in regulating cell growth and metabolism [14, 15]. Therefore, MSC-exo may affect the development of IUA and endometrial fibrosis through miRNAs. For instance, miR-29a in bone marrow MSC-exo can resist fibrosis during endometrial repair in IUA [16]. Moreover, miR-214-3p in exosomes can inhibit endometriosis fibrosis by targeting CCN2 [17]. Currently, systematic studies on the expression profile of miRNAs in MSC-exo are lacking, and the effect of key miRNAs on endometrial fibrosis and their regulatory mechanisms have yet to be fully elucidated.

In this study, we isolated and identified MSC-exo and investigated their effects on proliferation, apoptosis, and fibrosis in human endometrial epithelial cells (hEECs). Considering the promoting role of TGF-β1 in fibrotic diseases, we performed small RNA sequencing in MSC-exo and TGF-β1-induced MSC-exo, followed by miRNA identification and screening for differentially expressed (DE) miRNAs. Lastly, we selected key miRNAs and conducted functional experiments to further reveal the molecular mechanisms underlying the pathogenesis of IUA and endometrial fibrosis.

Methods

Cell culture

MSCs and hEECs were purchased from BeNa Culture Collection (BNCC) Biotechnology Co. Ltd. MSCs were cultured in 90% MEM basic medium (C11095500BT; Gibco, USA), 10% fetal bovine serum (FBS) (10099141; Gibco, USA), and 1% penicillin-streptomycin (15140-122; Gibco, USA). hEECs were maintained in DMEM-H complete medium (BNCC338068; BNCC, China) containing 10% FBS. The cell culture conditions were maintained at 37°C with 5% CO_2.

Preparation and isolation of exosomes

MSC were routinely grown and mass-expanded in an incubator at 37°C with 5% CO_2, whereas cells were cultured in MEM complete medium prepared with exosome-depleted FBS (EXO-FBS-50A-1; Systembio, USA). Once the density of adherent cells reached 80%, the cells were treated with 10 ng/ml TGF-β1 (ab50038; Abcam, Cambridge, UK) for 48 h, followed by the collection of the culture supernatant was collected. TGF-β1 was not added to the supernatant of the control group. MSC-exo were then collected by cryogenic hypervelocity centrifugation. To further identify the isolated MSC-exo, we first extracted their proteins for concentration determination and then detected the expression of exosome marker proteins (CD63 and HP70) using western blotting. Furthermore, the diluted MSC-exo were added to a Malvern NanoSight (NS300; Malvern, UK), and nanoparticle tracking analysis (NTA) was used to determine the particle size and concentration of MSC-exo.

Co-culture of MSCs and hEECs

To investigate the effect of MSC-exo on hEECs, MSCs and hEECs were co-cultured in a 6-well plate with a pore size of 0.4 μM at a ratio of 1:5. The group settings are presented in **Table 1**. hEECs were harvested after 24 and 48 h of co-culture for subsequent *in vitro* experiments.

CCK-8 assay

Fresh serum-free medium (500 μL) containing 10% 5 mg/mL CCK-8 solution (C0039; Beyotime Biotechnology, China) was added to the plate. After incubation in the dark for 1 h, the

Table 1. Conditions for co-culture of MSCs and hEECs in each experimental group

Group	Reagent	Upper layer	Under layer
1	Medium	/	hEECs
2	Medium + 10 ng/mL TGF-β1	/	hEECs
3	Medium + 10 ng/mL TGF-β1	MSCs	hEECs
4	Medium + 10 ng/mL TGF-β1 + 10 μM GW4869	MSCs	hEECs
5	Medium + 10 ng/mL TGF-β1 + 2 × 10^8/mL TGF-β1-induced MSC-exo	/	hEECs

MSC, mesenchymal stem cell; hEEC, human endometrial epithelial cell; MSC-exo, MSC-derived exosomes. GW4869 (HY-19363, MedChemExpress, USA) is the exosome inhibitor.

liquid in each well was aspirated and added to a 96-well plate at 100 μL/well, with five-well repeats. The absorbance of each well was measured at 450 nm using a microplate reader, and the cell survival rate was calculated.

Flow cytometry

Harvested cells were stored in 1.5-mL EP tubes and washed with 1 mL of PBS. After centrifugation at 1200 rpm for 3 min, the supernatant was discarded and the cells were resuspended in diluted binding buffer. Sample preparation was performed using an AnnexinV-PE/7-AAD Apoptosis Kit (88-8102-74; BD, USA). In the experimental group, 5 μL of PE-annexin V and 5 μL of 7-AAD (50 μg/mL) were added. Control cells were divided into a non-staining group, single-stained PE-annexin V group, single-stained 7-AAD group, and double-stained PE-annexin V + 7-AAD group. The prepared cells were then mixed and incubated for 15 min at room temperature in the dark. Lastly, the apoptosis of cells in each group was detected by flow cytometry (FACSCanto II; BD, USA).

Western blotting

Western blot experiments were performed according to the standard procedure. The primary antibodies used in this study, including anti-CD63 (ab252919; Abcam), anti-HSP70 (WL01019; Wanleibio, China), anti-α-SMA (ab-32575; Abcam, UK), anti-collagen I (WL0088; Wanleibio, China), anti-P62/SQSTM1 (66184-1-Ig; Proteintech, USA), and anti-GAPDH (60004-1-Ig; Proteintech, USA), were diluted at a concentration of 1:1000. The dilution concentrations of the secondary antibodies, namely Peroxidase AffiniPure Goat Anti-Rabbit IgG (H + L) (111-035-045; Jackson, USA) and Peroxidase AffiniPure Goat Anti-Mouse IgG (H + L) (115-035-003; Jackson, USA), were 1:10000 and 1:500, respectively. After antibody incubation and membrane washing, chemiluminescence was performed using a Millipore ECL System (Merck, USA). The final strips were collected using TanonImage (4600; Tanon, China) for data acquisition and gray-value analysis.

RNA-sequencing of small RNAs

MSC-exo and TGF-β1-induced MSC-exo (three samples for each group) were used for the high-throughput sequencing of small RNA using Illumina HiSeq. The original FASTQ file data were processed by primer and connector sequence removal, followed by quality control and length screening of sequencing fragments to select sequencing fragments with reliable quality. Clean reads obtained were sequentially aligned with the Rfam database [18], cDNA sequence, and species repetitive sequence library [19] to annotate the species of small RNA to obtain the sequence information of miRNA.

Bioinformatic analysis

Based on the identified miRNA expression levels, DESeq2 (version 1.16.1) [20, 21] was used to screen for DE miRNAs between the two groups. Then, miRanda [22] was used to predict the target genes of these DE miRNAs and to construct an miRNA-mRNA regulatory network. ClusterProfiler [23] was used to predict the Gene Ontology (GO) functions and Kyoto Encyclopedia of Genes and Genomes (KEGG) pathways of mRNAs in this network. The interactions between proteins encoded by the target genes were analyzed using STRING (version 11.5) [24]. The protein-protein interaction (PPI) network was constructed with a PPI score of 0.7 as threshold and visualized using Cytoscape (version 3.6.1) [25].

Reverse transcription-polymerase chain reaction (RT-PCR)

Based on the miRNA-mRNA regulatory network, we selected three key miRNAs to verify their mRNA expression levels. Total RNA was extracted from MSC-exo and TGF-β1-induced MSC-exo, followed by reverse transcription and amplification. The relative expression levels were calculated using $2^{-\Delta\Delta Ct}$ analysis. The primers for candidate miRNAs were as follows: hsa-miR-486-3p: CGCGGGGCAGCTCAGTA (forward) and AGTGCAGGGTCCGAGGTATT (reverse); hsa-miR-145-5p: CGGTCCAGTTTTCCCAGGA (forward) and AGTGCAGGGTCCGAGGTATT (reverse); hsa-miR-103b: CGCGTCATAGCCCTGTACAAT (forward) and AGTGCAGGGTCCGAGGTATT (reverse).

Cell transfection

To further explore the role of the key miRNAs in exosomes on IUA, TGF-β1 was used to induce hEECs to achieve fibrosis characteristics of the disease. Subsequently, the TGF-β1-induced hEECs were transfected with miR-145-5p mimic (5'-rGrUrCrCrArGrUrUrUrUrCrCrCrArGrGrArArUrCrCrCrU-3') to simulate the increased expression of exogenous miR-145-5p. The functional role of the candidate miRNAs was explored by testing the expression of fibrotic proteins (α-SMA and collagen I) and key autophagy proteins (P62) using western blotting.

Statistical analysis

All experiments were performed in triplicate, and the results are presented as the mean ± standard deviation. Statistical data were processed and plotted using GraphPad Prism5. Comparisons between multiple groups were analyzed using two-way ANOVA, while comparisons between two groups were performed using a *t* test. DE miRNAs between MSC-exo and TGF-β1-induced MSC-exo were screened with the threshold of $|\log_2 \text{fold change (FC)}| > 1$. The *p*-value was adjusted using the Benjamini-Hochberg (BH) method. In the GO and KEGG enrichment analyses, terms with a gene count > 2 were considered valid results. Statistical significance was set at p or adj. $P < 0.05$.

Results

Isolation and identification of MSC-exo

In this study, the protein marker expression and particle size of exosomes were first identified to confirm whether the isolated MSC-exo conformed to the basic characteristics. The western blotting results indicated that the exosome marker proteins CD63 and HSP70 were expressed in both MSC-exo- and TGF-β1-induced MSC-exo (**Figure 1A**). The original blots shown in **Figure 1A** are shown in Supplementary Figure 1. The particle sizes of MSC-exo and TGF-β1-induced MSC-exo were 179.0 ± 78.8 nm and 175.4 ± 59.5 nm, respectively (**Figure 1B**), which corresponded to the size standard of exosomes. These results confirmed the biologic characteristics of the isolated exosomes for use in subsequent experiments.

Effects of TGF-β1-induced MSC-exo on proliferation, apoptosis, and fibrosis of hEECs

TGF-β1 plays a key role in the epithelial-mesenchymal transition (EMT) of hEECs. In this study, the CCK-8 assay revealed that 24 and 48 h after TGF-β1 stimulation, the proliferation of hEECs was significantly inhibited. However, this inhibition was reversed when MSC and TGF-β1-induced MSC-exo were further appended, and cell proliferation showed significantly increasing trends in groups 3 and 5 compared to group 2 (**Figure 2A**). The results of flow cytometry suggested that the apoptosis of hEECs induced by TGF-β1 (group 2) was significantly higher than that of the control (group 1). However, in the co-culture of MSC (group 3) and TGF-β1-induced MSC-exo (group 5), apoptosis was significantly reduced compared to that in group 2 (**Figure 2B**). To further observe the degree of fibrosis in hEECs, the protein expression levels of Collagen 1 and α-SMA were detected by western blotting (**Figure 2C**). The expression levels of collagen 1 and α-SMA in TGF-β1-induced hEECs (group 2) were significantly higher than those in group 1. After the addition of MSC and TGF-β1-induced MSC-exo, the abnormally increased protein levels were significantly inhibited, and the expression of collagen 1 and α-SMA was significantly decreased in groups 3 and 5 compared to group 2. The original blots shown in **Figure 2C** are shown in Supplementary Figure 2. These findings indicate that TGF-β1 inhibited cell proliferation and promoted apoptosis and fibrosis in hEECs, while TGF-β1-induced MSC-exo significantly reversed these effects.

Small RNA sequencing of exosomes and sequence alignment annotation

To further explore the potential regulatory mechanism of exosomes on hEECs, we sequenced

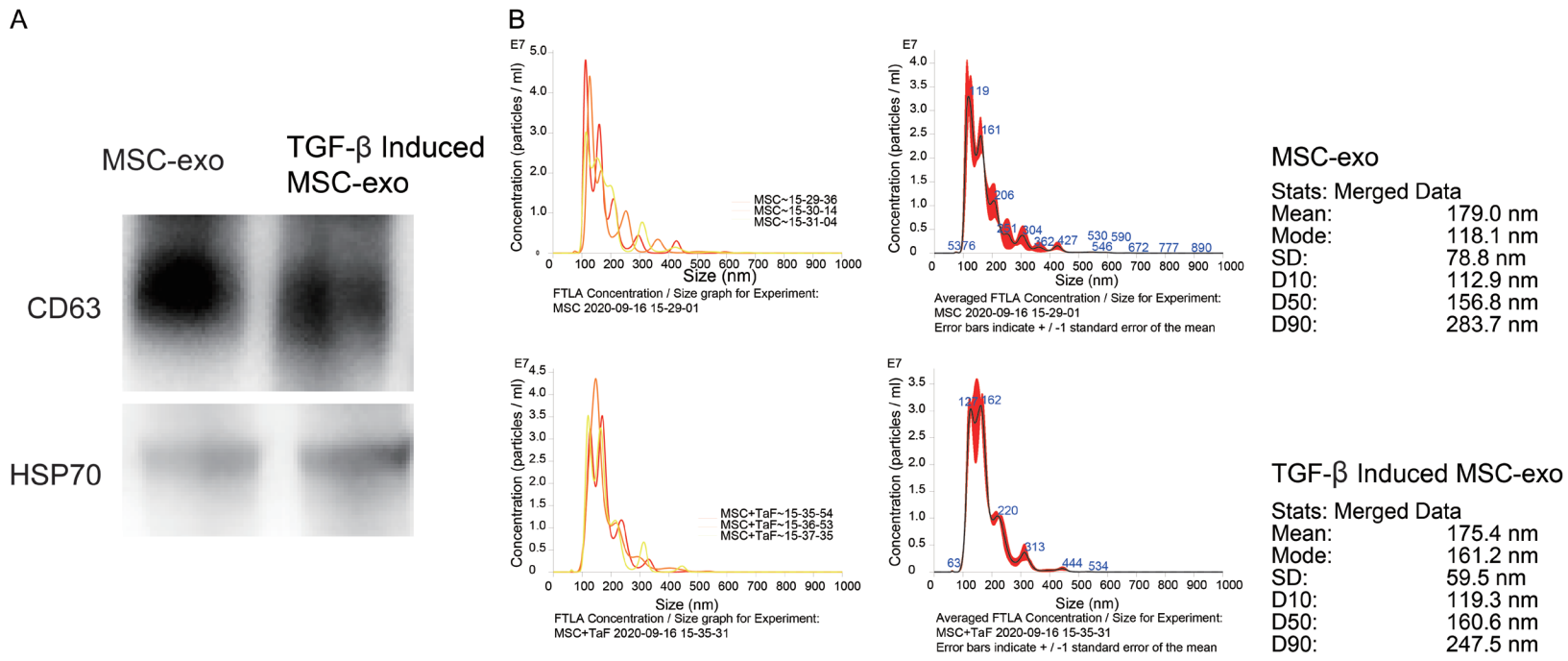

Figure 1. Basic characteristics of isolated mesenchymal stem cell-derived exosomes (MSC-exo). A: Expression of the marker proteins CD63 and HSP70 in MSC-exo and TGF-β1-induced MSC-exo. B: Particle sizes of isolated MSC-exo and TGF-β1-induced MSC-exo.

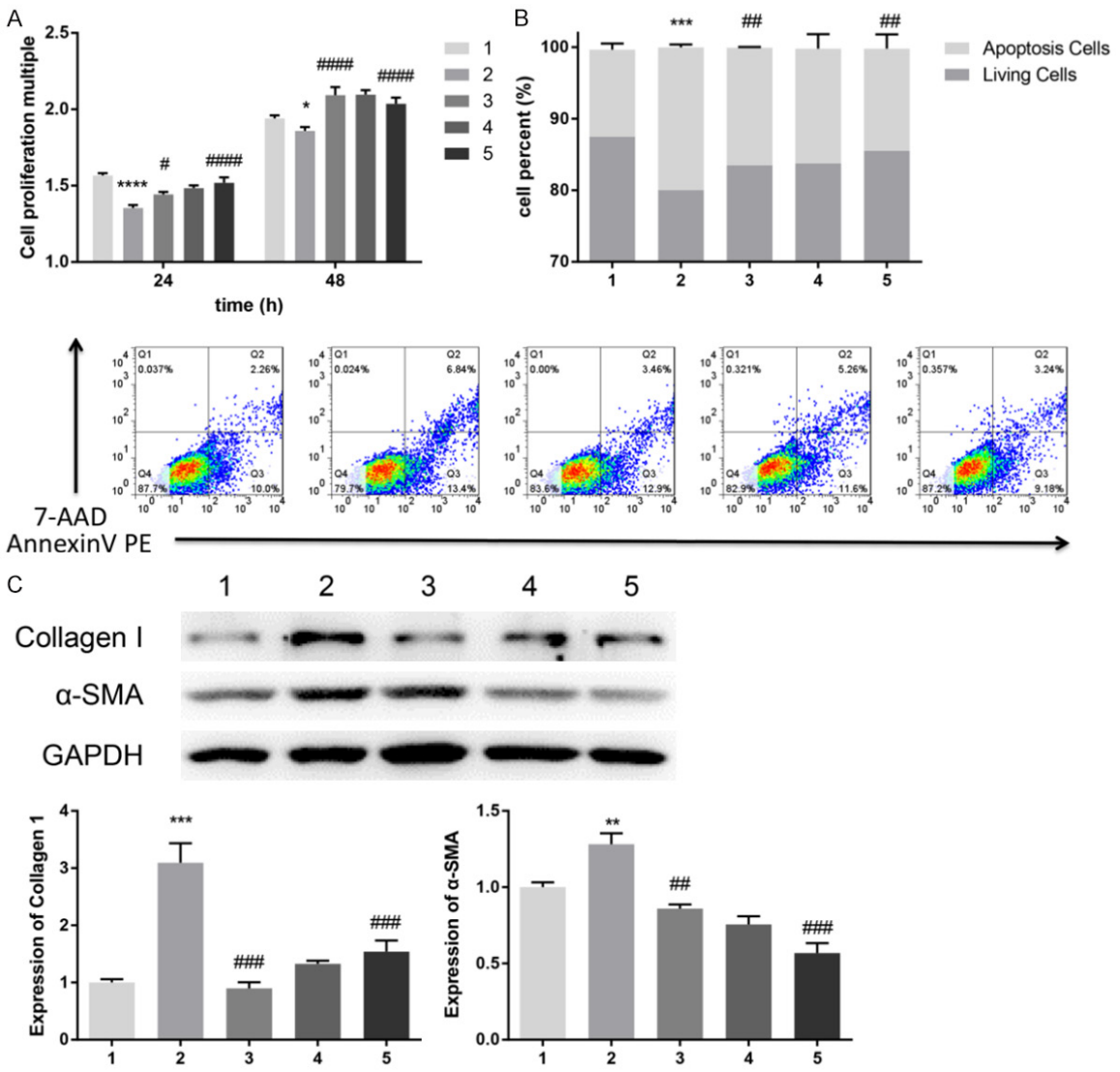

Figure 2. Effects of TGF-β1-induced mesenchymal stem cell-derived exosomes on proliferation, apoptosis, and fibrosis in human endometrial epithelial cells (hEECs). A: Proliferation of hEECs in the five groups at 24 and 48 h after TGF-β1 stimulation. B: Apoptosis of hEECs in all five groups was detected by flow cytometry. C: Western blot analysis revealed the expression levels of key proteins in fibrosis progression (collagen 1 and α-SMA) in hEECs of each group. *compared to group 1: $^{*}P < 0.05$, $^{**}P < 0.01$, $^{***}P < 0.001$, $^{****}P < 0.0001$. #compared with group 2: $^{\#}P < 0.05$, $^{\#\#}P < 0.01$, $^{\#\#\#}P < 0.001$, $^{\#\#\#\#}P < 0.0001$.

the small RNA of MSC-exo and TGF-β1-induced MSC-exo, and focused on the annotation and analysis of miRNAs. Each group contains three samples, wherein the distribution of clean reads of each sample ranged from 24.26 M to 28.05 M after data preprocessing. With the annotation of these clean reads, it was found that the genome alignment ranged from 24.52% to 56.17%, and the sRNAs in each sample mainly contained rRNAs, tRNAs, snRNAs, and miRNAs (**Figure 3A**). The miRNA alignment rate ranged from 0.02% to 0.05%, and the lengths were distributed in the range of 20-23 nt (**Figure 3B**). In addition, 427 miRNAs were identified in this study, and the number of miRNAs in each sample ranged from 176 to 237 (**Figure 3C**). Principal component analysis (PCA) (**Figure 3D**) indicated that the expression levels of these miRNAs could significantly separate MSC-exo and TGF-β1-induced MSC-exo samples, indicative of the high reliability of the data.

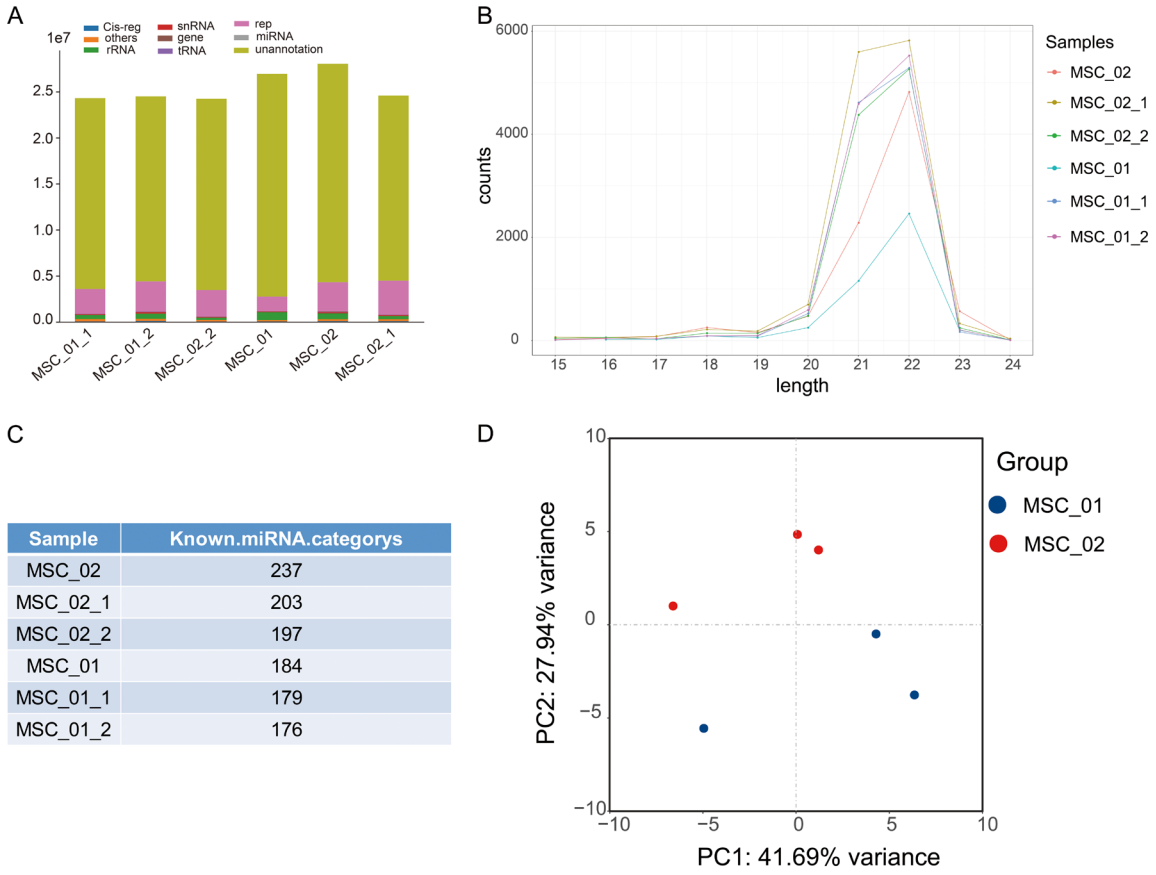

C

Sample	Known.miRNA.categorys
MSC_02	237
MSC_02_1	203
MSC_02_2	197
MSC_01	184
MSC_01_1	179
MSC_01_2	176

Figure 3. Sequencing alignment annotations of mesenchymal stem cell-derived exosomes (MSC-exo) and TGF-β1-induced MSC-exo samples. A: Clean reads from all samples were annotated and categorized. B: Line diagram of the length distribution of the matched microRNAs (miRNAs). C: The number of miRNAs identified in each sample. D: Principal component analysis of each sample based on miRNA expression levels.

Screening of DE miRNAs between MSC-exo and TGF-β1-induced MSC-exo

By comparing the expression profiles of miRNAs between MSC-exo and TGF-β1-induced MSC-exo, a total of 15 DE miRNAs were identified with the thresholds of BH-adjusted $P < 0.05$ and $|\log_2 FC| > 1$ (**Figure 4A**, **4B**). Of these, six miRNAs were upregulated and nine were downregulated. Heatmap analysis also confirmed that the expression patterns of these 15 DE miRNAs were significantly different between the two groups (**Figure 4C**).

Target gene prediction of DE miRNAs and enrichment analysis

To predict the target genes of the 15 DE miRNAs, we applied miRanda and constructed an miRNA-mRNA network comprising 10 DE miRNAs and 450 target genes (**Figure 5A**). These mRNAs were mainly involved in the biological processes of autophagy and process utilizing autophagic mechanism (**Figure 5B**), cell component of transferase complex, transferring phosphorus-containing groups (**Figure 5C**), and molecular function of SH3 domain binding (**Figure 5D**), as well as KEGG pathways of viral carcinogenesis, human virus infection, and PI3K-Akt signaling pathway (**Figure 5E**). Furthermore, this study constructed a PPI network, and the encoded proteins of 126 mRNAs were found to interact with each other (**Figure 5F**). *AGRN*, *SMAD3*, *EIF4G1*, *AXIN1*, and *ERBB2* may play critical roles in this network, as they exhibited a greater degree of connection.

Effects of miR-145-5p on IUA

Based on the miRNA-mRNA network constructed above, miR486-3p, miR-145-5p, and miR-103b, with more connections with target genes,

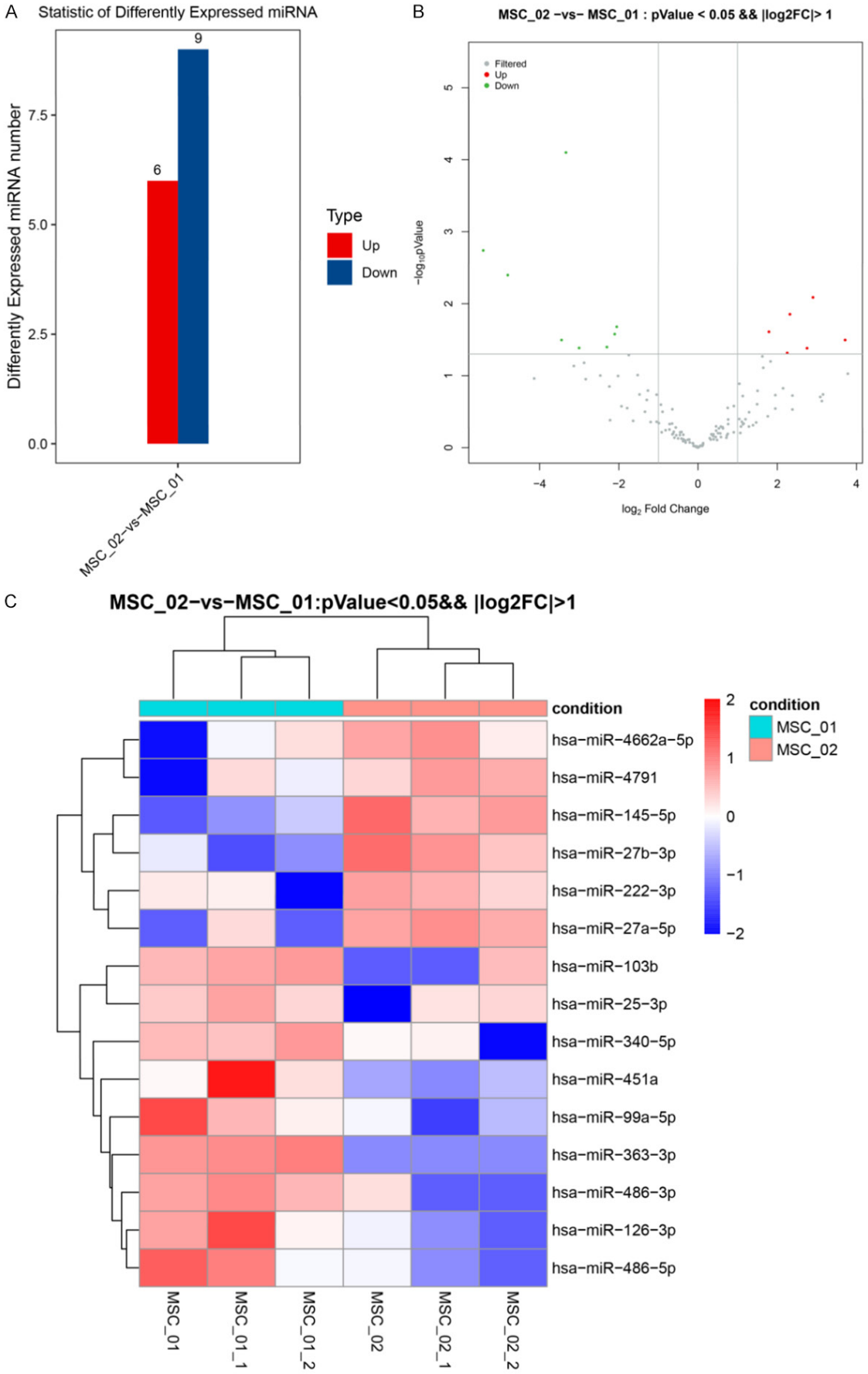
A
Statistic of Differently Expressed miRNA
Differently Expressed miRNA number
9
6
7.5
5.0
2.5
0.0
Type
Up
Down
MSC_02−vs−MSC_01
B
MSC_02 −vs− MSC_01 : pValue < 0.05 && |log2FC|> 1
Filtered
Up
Down
−log10pValue
log2 Fold Change
C
MSC_02−vs−MSC_01:pValue<0.05&& |log2FC|>1
condition
MSC_01
MSC_02
hsa−miR−4662a−5p
hsa−miR−4791
hsa−miR−145−5p
hsa−miR−27b−3p
hsa−miR−222−3p
hsa−miR−27a−5p
hsa−miR−103b
hsa−miR−25−3p
hsa−miR−340−5p
hsa−miR−451a
hsa−miR−99a−5p
hsa−miR−363−3p
hsa−miR−486−3p
hsa−miR−126−3p
hsa−miR−486−5p
MSC_01
MSC_01_1
MSC_01_2
MSC_02
MSC_02_1
MSC_02_2

Figure 4. Screening of differentially expressed (DE) microRNAs (miRNAs) between mesenchymal stem cell-derived exosomes (MSC-exo) and TGF-β1-induced MSC-exo samples. A: Histogram showing the number of DE miRNAs in the two groups. B: The volcano plot shows DE miRNAs that are upregulated and downregulated under the thresholds of adj. $P < 0.05$ and $|\log_2 \text{fold change}| > 1$. C: Heatmap showing differences in the expression patterns of these 15 DE miRNAs between the two groups.

were considered possible hub miRNAs and were verified by RT-PCR at the mRNA expression level. Only miR-145-5p showed significantly increased expression in TGF-β1-induced MSC-exo (**Figure 6A**). To further investigate the role of miR-145-5p, miR-145-5p mimics were transfected into hEECs. The western blotting results indicated that TGF-β1 induced hEECs exhibited more significant fibrosis features, including elevated protein expression levels of α-SMA and collagen I, as well as decreased expression of autophagy-related protein P62 (**Figure 6B**). However, with the addition of miR-145-5p mimics in TGF-β1-induced hEECs, the increased expression of α-SMA and collagen I and the decreased expression of P62 were all significantly reversed (**Figure 6B**). The original blots of **Figure 6B** are shown in Supplementary Figure 3. These results suggested that miR-145-5p in exosomes may alleviate the fibrotic characteristics of IUA by activating P62-dependent autophagy.

Discussion

TGF-β1 functions in the formation of IUA, and its expression level is significantly increased in patients with IUA, which is consistent with disease progression [26]. TGF-β1 also plays an important role in endometrial fibrosis induction. Studies have found that TGF-β1 is upregulated and activated in fibrotic diseases, regulates fibroblast phenotype and function, induces myofibroblast transdifferentiation, and promotes matrix preservation [27]. In the present study, TGF-β1 was used to stimulate hEECs *in vitro*. The proliferation of hEECs was found to be significantly inhibited, whereas the degrees of apoptosis and fibrosis were significantly increased. However, further addition of MSC and TGF-β1-induced MSC-exo improved the proliferation inhibition and fibrosis activation in hEECs. Liao et al. further confirmed our findings and suggested that MSC-exo could ameliorate reproductive disorders in women and exert therapeutic effects through mechanisms, such as angiogenesis, immune regulation, anti-fibrosis, and anti-oxidative stress [28]. Zhao et al. also found that adipose MSC-exo maintained normal uterine structure and promoted endometrial regeneration and fertility recovery in rats [29]. Furthermore, MSC-exo can reverse epithelial EMT and promote the repair of damaged endometria in rabbits [30]. Therefore, we concluded that MSC and MSC-exo can reverse endometrial fibrosis induced by TGF-β1; however, the regulatory mechanism remains to be elucidated.

To further explore the role of miRNAs in MSC-exo in endometrial fibrosis, we compared the miRNA expression profiles of MSC-exo and TGF-β1-induced MSC-exo and identified 15 DE miRNAs. Among these, miR-486-3p, miR-145-5p, and miR-103b may play important roles in the miRNA-mRNA regulatory network. Subsequent experimental verification further confirmed the increased expression of miR-145-5p in TGF-β1-induced MSC-exo. Exosome-derived miR-145-5p plays a functional role. MSC-exo have been reported to rescue skeletal muscle atrophy *in vivo* and *in vitro* in a miR-145-5p-dependent manner [31]. MSC-exo containing miR-145-5p attenuates the inflammatory response in spinal cord injury by regulating the TLR4/NF-κB signaling pathway [32]. Human umbilical cord MSC-exo transmits exogenous miR-145-5p to inhibit pancreatic ductal adenocarcinoma cell proliferation and invasion *in vitro* [33]. Therefore, we hypothesized that miR-145-5p in MSC-exo plays a protective role in ameliorating the inflammatory and tumor malignant phenotypes and that miR-145-5p expression is significantly increased in MSC-exo under TGF-β1 induction.

This study also found that TGF-β1 induced fibrosis in hEECs, and the addition of miR-145-5p mimics not only reversed the increased expression of fibrotic proteins but also significantly promoted the expression of the autophagy-related protein P62. Li et al. further confirmed our findings and proposed that umbilical cord MSC-exo reversed endometrial fibrosis through the miR-145-5p/ZEB2 axis in IUA [34]. Autophagy contributes to the progression of endometrial fibrosis in patients with IUA.

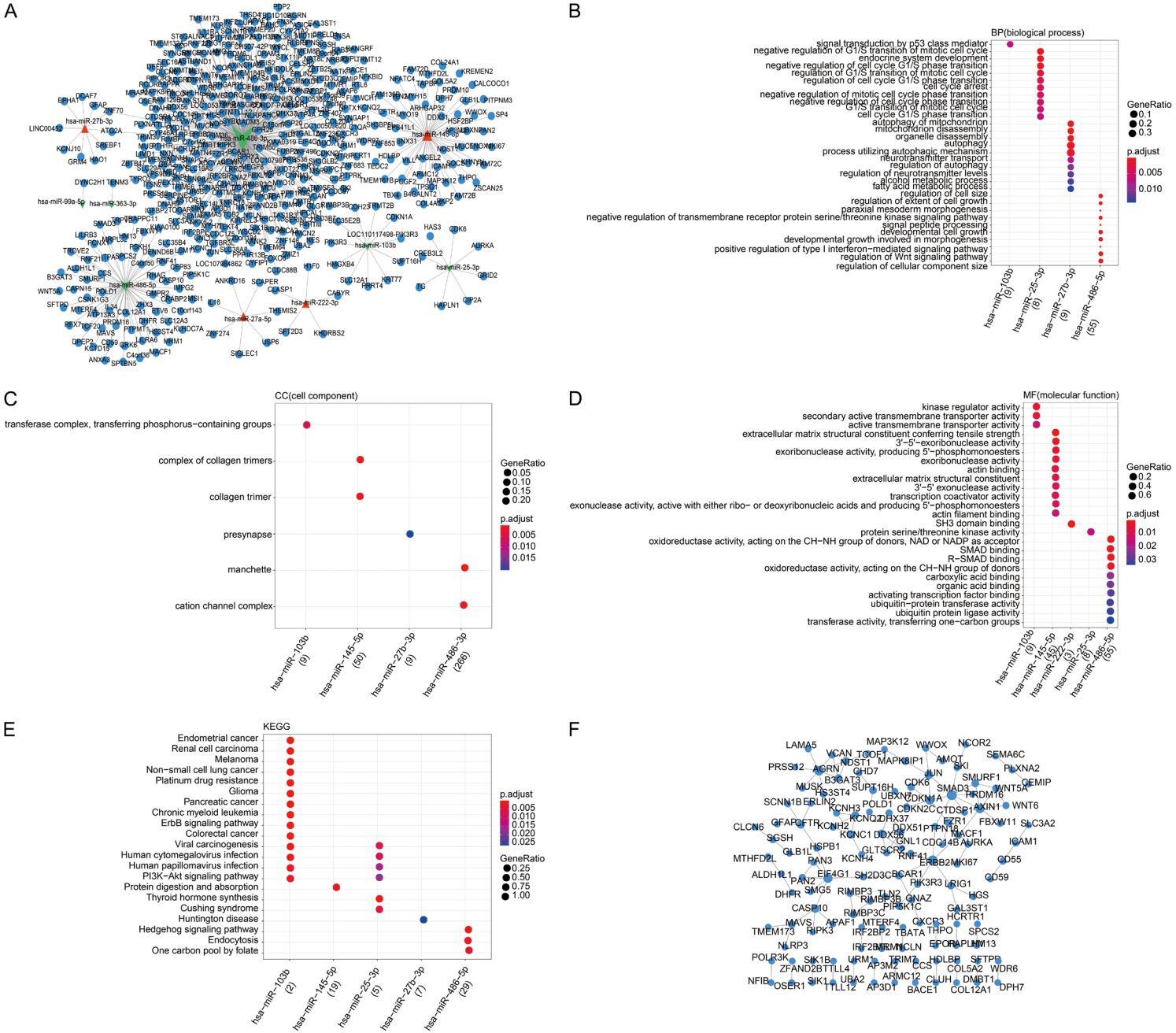
A
B
BP(biological process)
signal transduction by p53 class mediator
negative regulation of G1/S transition of mitotic cell cycle
endocrine system development
negative regulation of cell cycle G1/S phase transition
regulation of G1/S transition of mitotic cell cycle
regulation of cell cycle G1/S phase transition
cell cycle arrest
negative regulation of mitotic cell cycle phase transition
negative regulation of cell cycle phase transition
G1/S transition of mitotic cell cycle
cell cycle G1/S phase transition
autophagy of mitochondrion
mitochondrion disassembly
organelle disassembly
autophagy
process utilizing autophagic mechanism
neurotransmitter transport
regulation of autophagy
regulation of neurotransmitter levels
alcohol metabolic process
fatty acid metabolic process
regulation of cell size
regulation of extent of cell growth
paraxial mesoderm morphogenesis
negative regulation of transmembrane receptor protein serine/threonine kinase signaling pathway
signal peptide processing
developmental cell growth
developmental growth involved in morphogenesis
positive regulation of type I interferon−mediated signaling pathway
regulation of Wnt signaling pathway
regulation of cellular component size
GeneRatio
0.1
0.2
0.3
p.adjust
0.005
0.010
hsa−miR−103b (9)
hsa−miR−25−3p (6)
hsa−miR−27b−3p (9)
hsa−miR−486−5p (55)
C
CC(cell component)
transferase complex, transferring phosphorus−containing groups
complex of collagen trimers
collagen trimer
presynapse
manchette
cation channel complex
GeneRatio
0.05
0.10
0.15
0.20
p.adjust
0.005
0.010
0.015
hsa−miR−103b (9)
hsa−miR−145−5p (59)
hsa−miR−27b−3p (9)
hsa−miR−486−3p (266)
D
MF(molecular function)
kinase regulator activity
secondary active transmembrane transporter activity
active transmembrane transporter activity
extracellular matrix structural constituent conferring tensile strength
3′−5′−exoribonuclease activity
exoribonuclease activity, producing 5′−phosphomonoesters
exoribonuclease activity
actin binding
extracellular matrix structural constituent
3′−5′ exonuclease activity
transcription coactivator activity
exonuclease activity, active with either ribo− or deoxyribonucleic acids and producing 5′−phosphomonoesters
actin filament binding
SH3 domain binding
protein serine/threonine kinase activity
oxidoreductase activity, acting on the CH−NH group of donors, NAD or NADP as acceptor
SMAD binding
R−SMAD binding
oxidoreductase activity, acting on the CH−NH group of donors
carboxylic acid binding
organic acid binding
activating transcription factor binding
ubiquitin−protein transferase activity
ubiquitin protein ligase activity
transferase activity, transferring one−carbon groups
GeneRatio
0.2
0.4
0.6
p.adjust
0.01
0.02
0.03
hsa−miR−103b (9)
hsa−miR−145−5p (59)
hsa−miR−27b−3p (9)
hsa−miR−25−3p (6)
hsa−miR−486−5p (55)
E
KEGG
Endometrial cancer
Renal cell carcinoma
Melanoma
Non−small cell lung cancer
Platinum drug resistance
Glioma
Pancreatic cancer
Chronic myeloid leukemia
ErbB signaling pathway
Colorectal cancer
Viral carcinogenesis
Human cytomegalovirus infection
Human papillomavirus infection
PI3K−Akt signaling pathway
Protein digestion and absorption
Thyroid hormone synthesis
Cushing syndrome
Huntington disease
Hedgehog signaling pathway
Endocytosis
One carbon pool by folate
p.adjust
0.005
0.010
0.015
0.020
0.025
GeneRatio
0.25
0.50
0.75
1.00
hsa−miR−103b (2)
hsa−miR−145−5p (19)
hsa−miR−25−3p (5)
hsa−miR−27b−3p (7)
hsa−miR−486−5p (29)
F

Figure 5. Prediction of target genes of differentially expressed (D, E) microRNAs (miRNAs) followed by gene ontology (GO) and Kyoto Encyclopedia of Genes and Genomes (KEGG) enrichment analyses. (A) Construction of a miRNA-mRNA regulatory network containing 10 DE miRNAs and 450 target genes. (B-E) GO function in terms of biological processes (B), cell components (C), and molecular functions (D), as well as KEGG pathway (E) enrichment analyses of target genes. (F) Generation of a protein-protein interaction network based on the DE miRNA target genes.

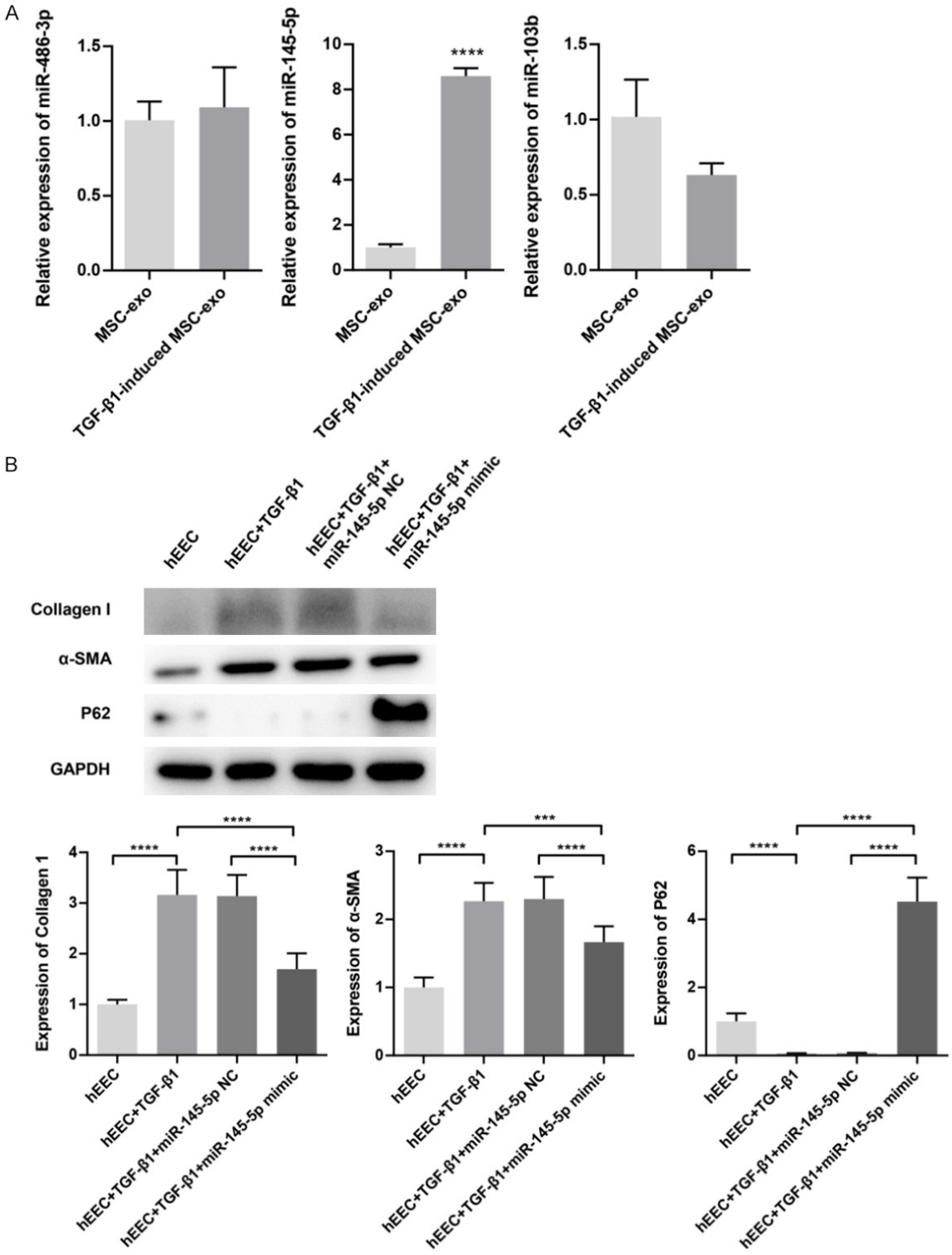

Figure 6. Expression verification of key microRNAs and functional investigation. A: Differences in the relative mRNA expression of miR-486-3p, miR-145-5p, and miR-103b between mesenchymal stem cell-derived exosomes (MSC-exo) and TGF-β1-induced MSC-exo. $^{****}P < 0.0001$. B: Detection of changes in expression of fibrotic and autophagic proteins after transfecting miR-145-5p mimics into TGF-β1-induced human endometrial epithelial cells. $^{***}P < 0.001$, $^{****}P < 0.0001$.

Endometrial autophagy defects aggravate EMT and endometrial fibrosis in patients with IUA [35]. Li et al. also observed changes in autophagy in IUA mice, whereas the transplantation of human amniotic epithelial cells with stem cell properties upregulated autophagy and improved angiogenesis and stromal cell proliferation [36]. Our findings indicated that miR-145-5p may alleviate IUA fibrosis by activating P62-dependent autophagy. Furthermore, the circ-SIRT1/miR-145-5p/Akt3 regulatory axis was reported to regulate P62-mediated autophagy in rats with pulmonary hypertension [37]. In addition, the downregulation of miR-145-5p can activate autophagy in atherosclerosis by the AMPK/mTOR/ULK1 signaling pathway [38]. Both AMPK/mTOR and P62 are classical autophagic pathways, whereas SQSTM1/p62 can regulate the AMPK/mTOR pathway to promote tumor cell growth and trigger autophagy [39]. This study initially proposed associations between miR-145-5p and P62-dependent autophagy in IUA fibrosis; however, their upstream and downstream regulatory mechanisms require further investigation.

Despite confirming the role of MSC-exo in reversing endometrial fibrosis induced by TGF-β1, there remains a persistent lack of experimental studies on the regulatory mechanism of autophagy involving key miRNAs and target genes, which is the main limitation of this study. In subsequent studies, we hope to further confirm the targeted binding relationship between miR-145-5p and its downstream genes and refine the upstream and downstream regulatory mechanisms of miR-145-5p and P62-dependent autophagy through a series of *in vivo* and *in vitro* experiments.

Conclusion

In this study, MSC-exo were successfully isolated and identified, and were confirmed to reverse the effect of TGF-β1 on cell proliferation, apoptosis, and fibrosis in hEECs *in vivo*. After sequencing and comparing the miRNA expression profiles of MSC-exo and TGF-β1-induced MSC-exo, 15 DE miRNAs were identified. Of these, miR-145-5p was experimentally verified to be significantly upregulated in TGF-β1-induced MSC-exo and may reverse IUA fibrosis by activating P62-dependent autophagy.

Disclosure of conflict of interest

None.

Address correspondence to: Zhixin Huang and Jing Yang, Department of Obstetrics and Gynecology, Renmin Hospital of Wuhan University, No. 99 Zhang Zhidong Road, Wuchang District, Wuhan 430060, Hubei, China. Tel: +86-027-88041919; E-mail: huanjiu472qiaohuai@163.com (ZXH); dryangjing@whu.edu.cn (JY)

References

[1] Doroftei B, Dabuleanu AM, Ilie OD, Maftei R, Anton E, Simionescu G, Matei T and Armeanu T. Mini-review of the new therapeutic possibilities in asherman syndrome-where are we after one hundred and twenty-six years? Diagnostics (Basel) 2020; 10: 706.

[2] Kou L, Jiang X, Xiao S, Zhao YZ, Yao Q and Chen R. Therapeutic options and drug delivery strategies for the prevention of intrauterine adhesions. J Control Release 2020; 318: 25-37.

[3] Dreisler E and Kjer JJ. Asherman's syndrome: current perspectives on diagnosis and management. Int J Womens Health 2019; 11: 191-198.

[4] Lee WL, Liu CH, Cheng M, Chang WH, Liu WM and Wang PH. Focus on the primary prevention of intrauterine adhesions: current concept and vision. Int J Mol Sci 2021; 22: 5175.

[5] Capmas P, Mihalache A, Duminil L, Hor LS, Pourcelot AG and Fernandez H. Intrauterine adhesions: what is the pregnancy rate after hysteroscopic management? J Gynecol Obstet Hum Reprod 2020; 49: 101797.

[6] Santamaria X, Isaacson K and Simón C. Asherman's syndrome: it may not be all our fault. Hum Reprod 2018; 33: 1374-1380.

[7] Costa LA, Eiro N, Fraile M, Gonzalez LO, Saá J, Garcia-Portabella P, Vega B, Schneider J and Vizoso FJ. Functional heterogeneity of mesenchymal stem cells from natural niches to culture conditions: implications for further clinical uses. Cell Mol Life Sci 2021; 78: 447-467.

[8] Xin L, Lin X, Zhou F, Li C, Wang X, Yu H, Pan Y, Fei H, Ma L and Zhang S. A scaffold laden with mesenchymal stem cell-derived exosomes for

promoting endometrium regeneration and fertility restoration through macrophage immunomodulation. Acta Biomater 2020; 113: 252-266.
[9] Zhai M, Zhu Y, Yang M and Mao C. Human mesenchymal stem cell derived exosomes enhance cell-free bone regeneration by altering their mirnas profiles. Adv Sci (Weinh) 2020; 7: 2001334.
[10] Harrell CR, Fellabaum C, Jovicic N, Djonov V, Arsenijevic N and Volarevic V. Molecular mechanisms responsible for therapeutic potential of mesenchymal stem cell-derived secretome. Cells 2019; 8: 467.
[11] Xu S, Liu C and Ji HL. Concise review: therapeutic potential of the mesenchymal stem cell derived secretome and extracellular vesicles for radiation-induced lung injury: progress and hypotheses. Stem Cells Transl Med 2019; 8: 344-354.
[12] Lai RC, Yeo RW and Lim SK. Mesenchymal stem cell exosomes. Semin Cell Dev Biol 2015; 40: 82-88.
[13] Harrell CR, Jovicic N, Djonov V, Arsenijevic N and Volarevic V. Mesenchymal stem cell-derived exosomes and other extracellular vesicles as new remedies in the therapy of inflammatory diseases. Cells 2019; 8: 1605.
[14] Zhang J, Li S, Li L, Li M, Guo C, Yao J and Mi S. Exosome and exosomal microRNA: trafficking, sorting, and function. Genomics Proteomics Bioinformatics 2015; 13: 17-24.
[15] Yu X, Odenthal M and Fries JW. Exosomes as miRNA carriers: formation-function-future. Int J Mol Sci 2016; 17: 2028.
[16] Tan Q, Xia D and Ying X. miR-29a in exosomes from bone marrow mesenchymal stem cells inhibit fibrosis during endometrial repair of intrauterine adhesion. Int J Stem Cells 2020; 13: 414-423.
[17] Zhang Y, Chang X, Wu D, Deng M, Miao J and Jin Z. Down-regulation of exosomal miR-214-3p targeting CCN2 contributes to endometriosis fibrosis and the role of exosomes in the horizontal transfer of miR-214-3p. Reprod Sci 2021; 28: 715-727.
[18] Griffiths-Jones S, Bateman A, Marshall M, Khanna A and Eddy SR. Rfam: an RNA family database. Nucleic Acids Res 2003; 31: 439-441.
[19] Chen N. Using RepeatMasker to identify repetitive elements in genomic sequences. Curr Protoc Bioinformatics 2004; Chapter 4: Unit 4.10.
[20] Anders S. Analysing RNA-Seq data with the DESeq package. Mol Biol 2010; 43: 1-17.
[21] Love MI, Huber W and Anders S. Moderated estimation of fold change and dispersion for RNA-seq data with DESeq2. Genome Biol 2014; 15: 550.
[22] John B, Enright AJ, Aravin A, Tuschl T, Sander C and Marks DS. Human microRNA targets. PLoS Biol 2004; 2: e363.
[23] Yu G, Wang LG, Han Y and He QY. clusterProfiler: an R package for comparing biological themes among gene clusters. OMICS 2012; 16: 284-287.
[24] Szklarczyk D, Gable AL, Nastou KC, Lyon D, Kirsch R, Pyysalo S, Doncheva NT, Legeay M, Fang T, Bork P, Jensen LJ and von Mering C. The STRING database in 2021: customizable protein-protein networks, and functional characterization of user-uploaded gene/measurement sets. Nucleic Acids Res 2021; 49: D605-D612.
[25] Shannon P, Markiel A, Ozier O, Baliga NS, Wang JT, Ramage D, Amin N, Schwikowski B and Ideker T. Cytoscape: a software environment for integrated models of biomolecular interaction networks. Genome Res 2003; 13: 2498-2504.
[26] Xue X, Chen Q, Zhao G, Zhao JY, Duan Z and Zheng PS. The overexpression of TGF-β and CCN2 in intrauterine adhesions involves the NF-κB signaling pathway. PLoS One 2015; 10: e0146159.
[27] Wu D, Lu P, Mi X and Miao J. Exosomal miR-214 from endometrial stromal cells inhibits endometriosis fibrosis. Mol Hum Reprod 2018; 24: 357-365.
[28] Liao Z, Liu C, Wang L, Sui C and Zhang H. Therapeutic role of mesenchymal stem cell-derived extracellular vesicles in female reproductive diseases. Front Endocrinol (Lausanne) 2021; 12: 665645.
[29] Zhao S, Qi W, Zheng J, Tian Y, Qi X, Kong D, Zhang J and Huang X. Exosomes derived from adipose mesenchymal stem cells restore functional endometrium in a rat model of intrauterine adhesions. Reprod Sci 2020; 27: 1266-1275.
[30] Yao Y, Chen R, Wang G, Zhang Y and Liu F. Exosomes derived from mesenchymal stem cells reverse EMT via TGF-β1/Smad pathway and promote repair of damaged endometrium. Stem Cell Res Ther 2019; 10: 225.
[31] Cho KA, Choi DW, Kim YH, Kim J, Ryu KH and Woo SY. Mesenchymal stem cell-derived exosomes protect muscle loss by miR-145-5p activity targeting activin a receptors. Cells 2021; 10: 2169.
[32] Jiang Z and Zhang J. Mesenchymal stem cell-derived exosomes containing miR-145-5p reduce inflammation in spinal cord injury by regulating the TLR4/NF-κB signaling pathway. Cell Cycle 2021; 20: 993-1009.
[33] Ding Y, Cao F, Sun H, Wang Y, Liu S, Wu Y, Cui Q, Mei W and Li F. Exosomes derived from human umbilical cord mesenchymal stromal cells deliver exogenous miR-145-5p to inhibit

pancreatic ductal adenocarcinoma progression. Cancer Lett 2019; 442: 351-361.
[34] Li X, Duan H, Wang S and Lv CX. Umbilical cord mesenchymal stem cell-derived exosomes reverse endometrial fibrosis by the miR-145-5p/ZEB2 axis in intrauterine adhesions. Reprod Biomed Online 2023; 46: 234-243.
[35] Zhou Z, Wang H, Zhang X, Song M, Yao S, Jiang P, Liu D, Wang Z, Lv H, Li R, Hong Y, Dai J, Hu Y and Zhao G. Defective autophagy contributes to endometrial epithelial-mesenchymal transition in intrauterine adhesions. Autophagy 2022; 18: 2427-2442.
[36] Li B, Zhang Q, Sun J and Lai D. Human amniotic epithelial cells improve fertility in an intrauterine adhesion mouse model. Stem Cell Res Ther 2019; 10: 257.
[37] Jing X, Wu S, Liu Y, Wang H and Huang Q. Circular RNA Sirtuin1 represses pulmonary artery smooth muscle cell proliferation, migration and autophagy to ameliorate pulmonary hypertension via targeting microRNA-145-5p/protein kinase-B3 axis. Bioengineered 2022; 13: 8759-8771.
[38] Zhang X, Zai L, Tao Z, Wu D, Lin M and Wan J. miR-145-5p affects autophagy by targeting CaMKIIδ in atherosclerosis. Int J Cardiol 2022; 360: 68-75.
[39] Yu F, Ma R, Liu C, Zhang L, Feng K, Wang M and Yin D. SQSTM1/p62 promotes cell growth and triggers autophagy in papillary thyroid cancer by regulating the AKT/AMPK/mTOR signaling pathway. Front Oncol 2021; 11: 638701.

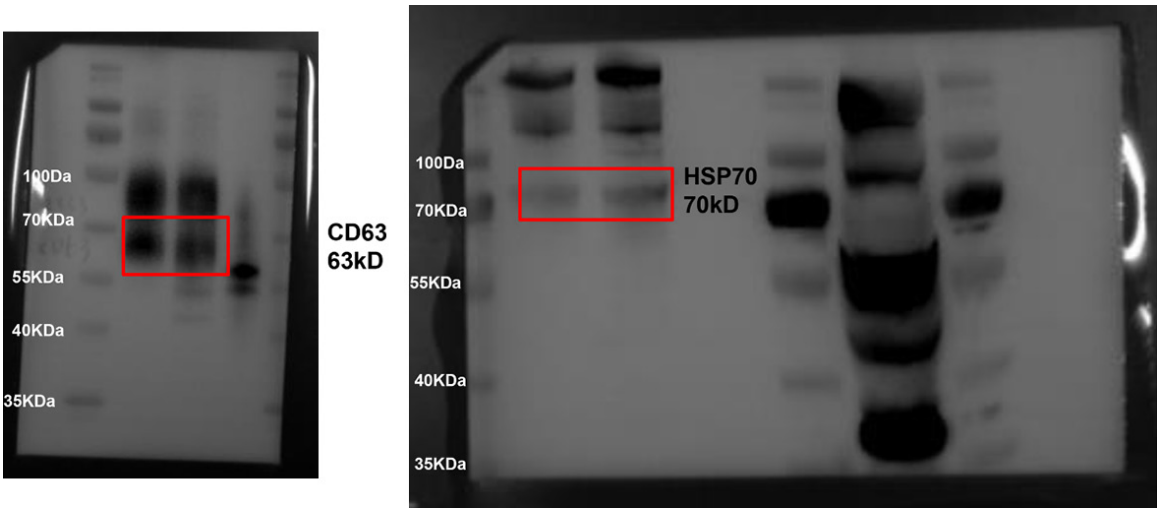

Supplementary Figure 1. Original and full-length blot images for the marker proteins CD63 and HSP70 in MSC-exo.

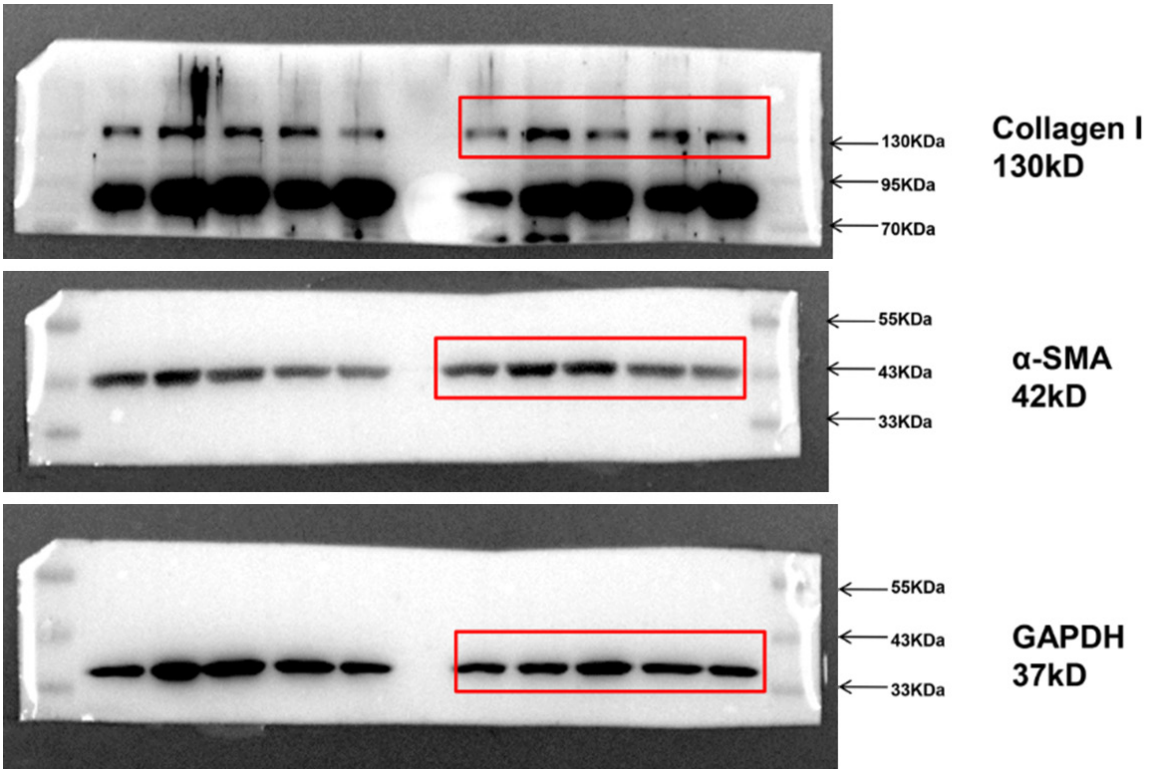

Supplementary Figure 2. Original and full-length blot images for collagen 1 and α-SMA in hEECs of each group.

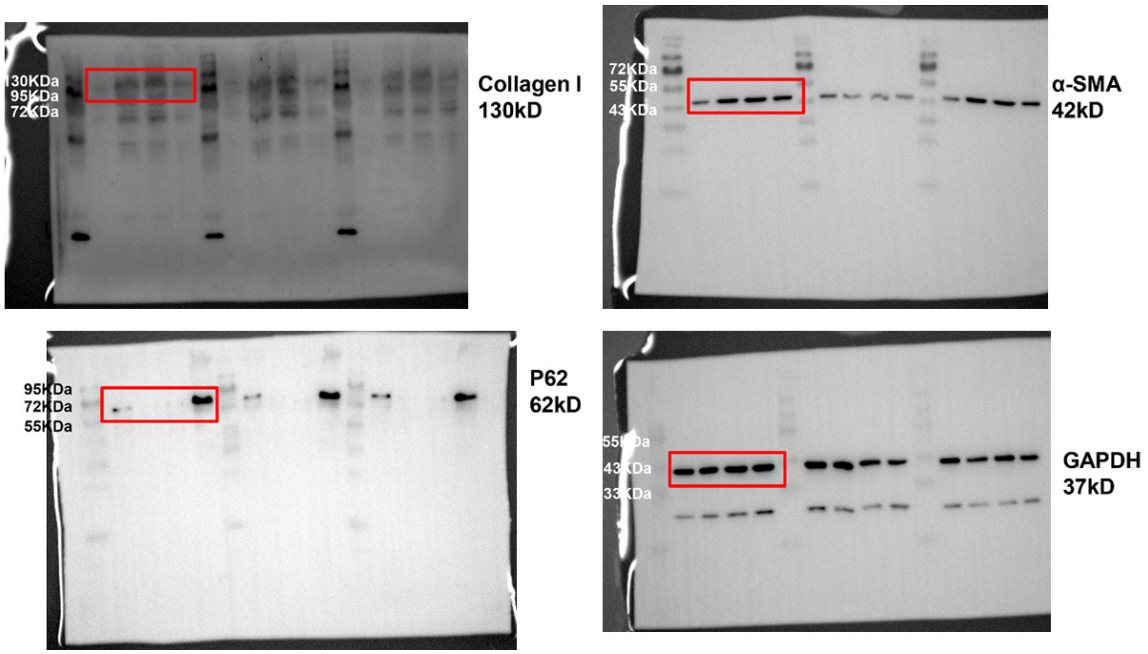

Supplementary Figure 3. Original and full-length blot images for changes in expression of fibrotic and autophagic proteins after transfecting miR-145-5p mimics into TGF-β1-induced human endometrial epithelial cells.